Formation and size distribution of self-assembled vesicles

Changjin Huang[a], David Quinn[b], Yoel Sadovsky[c,d,e], Subra Suresh[a,f,g,h,1], and K. Jimmy Hsia[a,b,1]

[a]Department of Biomedical Engineering, Carnegie Mellon University, Pittsburgh, PA 15213; [b]Department of Mechanical Engineering, Carnegie Mellon University, Pittsburgh, PA 15213; [c]Magee-Womens Research Institute, University of Pittsburgh, Pittsburgh, PA 15213; [d]Department of Obstetrics, Gynecology, and Reproductive Sciences, University of Pittsburgh, Pittsburgh, PA 15213; [e]Department of Microbiology and Molecular Genetics, University of Pittsburgh, Pittsburgh, PA 15219; [f]Department of Materials Science and Engineering, Carnegie Mellon University, Pittsburgh, PA 15213; [g]Department of Computational Biology, Carnegie Mellon University, Pittsburgh, PA 15213; and [h]School of Medicine, University of Pittsburgh, Pittsburgh, PA 15261

Contributed by Subra Suresh, February 7, 2017 (sent for review December 14, 2016; reviewed by Ashutosh Agrawal and Markus J. Buehler)

When detergents and phospholipid membranes are dispersed in aqueous solutions, they tend to self-assemble into vesicles of various shapes and sizes by virtue of their hydrophobic and hydrophilic segments. A clearer understanding of such vesiculation processes holds promise for better elucidation of human physiology and disease, and paves the way to improved diagnostics, drug development, and drug delivery. Here we present a detailed analysis of the energetics and thermodynamics of vesiculation by recourse to nonlinear elasticity, taking into account large deformation that may arise during the vesiculation process. The effects of membrane size, spontaneous curvature, and membrane stiffness on vesiculation and vesicle size distribution were investigated, and the critical size for vesicle formation was determined and found to compare favorably with available experimental evidence. Our analysis also showed that the critical membrane size for spontaneous vesiculation was correlated with membrane thickness, and further illustrated how the combined effects of membrane thickness and physical properties influenced the size, shape, and distribution of vesicles. These findings shed light on the formation of physiological extracellular vesicles, such as exosomes. The findings also suggest pathways for manipulating the size, shape, distribution, and physical properties of synthetic vesicles, with potential applications in vesicle physiology, the pathobiology of cancer and other diseases, diagnostics using in vivo liquid biopsy, and drug delivery methods.

extracellular vesicles | self-assembly | size distribution | exosome | large deformation

Natural and synthetic materials such as soaps, detergents, phospholipids, and block copolymers are not only ubiquitous, but they also play an essential role in research into human physiology and medicine (1–4) and in engineering of new materials and devices (5). These so-called amphiphiles comprise both hydrophobic and hydrophilic segments. When dispersed in aqueous solutions at a concentration above a threshold level known as the critical micelle concentration (CMC) (6), they self-assemble into aggregates of varying sizes and shapes, including unilamellar vesicles, micelles (spheres and tubes), and multilamellar compounds (6, 7). Analyses invoking considerations of the geometry of amphiphiles have enabled predictions of their aggregate configurations (8). Among all predicted and observed configurations, unilamellar vesicles have attracted special attention due to their scientific and clinical significance, a subset of which is found in the following examples:

i) Exosomes, the smallest members (30 nm to 150 nm in diameter) within the extracellular vesicle (EV) family, are known to influence intercellular communication (9–11). For example, the formation and release of exosomes from primary tumors may be uptaken by specific cells in specific destinations that regulate the metastatic niche in target organs (12). In human pregnancy, the analysis of placental EVs suggests that, despite comparable cargo comprising proteins, RNA, miRNA, lipids, and/or metabolites, trophoblastic exosomes confer a more potent viral resistance to target cells than larger trophoblastic microvesicles and apoptotic blebs (10, 13).

ii) Artificial unilamellar vesicles, formed via self-assembly of phospholipids or synthetic amphiphilic block copolymers, have been widely tested as drug carriers in cancer diagnosis and treatment (14, 15). The size and shape of vesicles are known to influence how effectively they are uptaken by cells (16–18). Therefore, tailoring vesicle size for optimal diagnostics, drug delivery, and therapeutics has the potential to improve clinical outcomes.

iii) Studies of endocytosis reveal a number of pathways and mechanisms by which EVs are internalized in diverse cell types, indicating that the vesicle's origin, size, and composition, as well as the type and growth status of the target cell (19), might determine vesicle–endocytosis mechanisms. Studies in this area may promote the innovative development of engineered nanovesicles or microvesicles to deliver molecules or drugs to specific tissues in a manner that mimics natural biological processes.

Vesiculation in aqueous solution is considered a spontaneous process driven by the minimization of the line energy that arises as a result of exposure of the nonpolar hydrophobic core to polar water molecules along the free edge of membrane patches. Only when the driving force is sufficiently high to overcome the corresponding bending resistance does the curving of a planar membrane patch into a sphere become possible, with the attendant formation of a vesicle of "minimal size" (14, 20). This rationale has been qualitatively confirmed by molecular dynamics (MD) simulations, in which vesiculation is observed only after membrane patches grow beyond

Significance

Small unilamellar vesicles formed via self-assembly of phospholipids or block copolymers have been investigated in the context of human physiology and biomedical research. Here, we present both energetics and thermodynamics analyses that incorporate nonlinear elasticity to predict, in a unique manner, the limiting size and size distribution of vesicles as well as to identify the conditions for the formation of stable open vesicles, disks, and closed spherical vesicles. In addition to providing a comprehensive understanding of vesicle formation, the framework presented here may be adapted to develop tools for in vivo liquid biopsies and to elucidate the biophysical features of extracellular vesicles, thus suggesting new approaches to diagnostics and therapeutics for cancer and other diseases.

Author contributions: S.S. and K.J.H. designed research; C.H. performed research; C.H. and D.Q. analyzed data; and C.H., D.Q., Y.S., S.S., and K.J.H. wrote the paper.

Reviewers: A.A., University of Houston; and M.J.B., Massachusetts Institute of Technology.

The authors declare no conflict of interest.

Freely available online through the PNAS open access option.

[1]To whom correspondence may be addressed. Email: kjhsia@cmu.edu or suresh@cmu.edu.

a critical size (21, 22). However, classical mechanics analyses (23, 24), which model the membrane as a sheet with zero thickness undergoing small, linear elastic local deformation, predict the self-assembly of either disks or closed spherical vesicles as stable configurations. Such an approach is somewhat limited in scope in that it is silent on the formation of many other configurations, such as open vesicles (25–27) and tubular vesicles (14, 28), the self-assembly of which have been demonstrated experimentally. Because the local radius of curvature of small unilamellar vesicles can be comparable to the membrane thickness, the classical approach could have serious limitations in its ability to faithfully predict the vesiculation of membranes of broad interest in biology (29, 30).

To address the limitations of this conventional model, the role of nonlinearity in membrane bending has been introduced in the analysis of vesiculation by incorporating curvature-dependent elastic parameters (31). Following this reasoning, it has been shown that the bending modulus of a 16-nm-diameter vesicle could be as much as 4 times higher than the modulus of its planar counterparts (32). An alternative approach is to include higher-order terms in the quadratic Helfrich bending energy (33, 34). When the fourth-order membrane bending terms are incorporated in energy minimization, it is found that experimental observations of the formation of tubular vesicles (35) and open vesicles (36) could be rationalized. When nonlinear curvature elasticity is incorporated into thermal fluctuation analysis, considerably higher bending moduli values are extracted for vesicles smaller than 20 nm in diameter (37).

Here we present detailed analyses of the energetics and thermodynamics of vesicle formation, by invoking nonlinear elasticity to model high-curvature membrane bending as well as configurational entropy associated with the vesicle formation process. This approach enables us to predict in a unique manner the limiting vesicle size and distribution of vesicle sizes as well as to identify the conditions and phase diagrams for the formation of stable open vesicles, disks, and closed spherical vesicles. The analysis also provides quantitative insights into the critical influence of membrane thickness and stiffness on vesicle shape and on vesicle size distribution. The analyses are discussed in the context of vesicle self-assembly in diverse biological situations, exploring possible avenues for the optimal design of synthetic vesicles in drug delivery applications.

Spontaneous Vesiculation

As suggested by both MD simulations (21, 22) and high temporal resolution X-ray scattering experiments (38), vesiculation starts from small aggregations of individual amphiphiles, which then grow into disk-like bilayer structures after they coalesce with one another and/or fuse with individual amphiphiles (Fig. 1*A*). As a bilayer structure grows, it generally seeks to maintain a circular patch configuration because the peripheral length of a circle is the smallest among all possible configurations for any given surface area, thereby minimizing the overall line energy. To further reduce the line energy, the bilayer structure tends to curve upon growing to a certain size (Fig. 1 *B* and *C*), and eventually closes to form a spherical vesicle, as shown in Fig. 1*D*.

The reduction in line energy during the transition from a planar patch to a closed vesicle is countered by an increase in the membrane bending energy. Although vesicle sizes largely depend on the kinetics of membrane size growth, there exists a critical membrane size below which vesicle formation is energetically unfavorable. Identification of this critical size would provide a better understanding of the final vesicle size distribution, especially its lower bound.

From an energetics point of view, vesiculation becomes spontaneous only if the system energy monotonically decreases as a

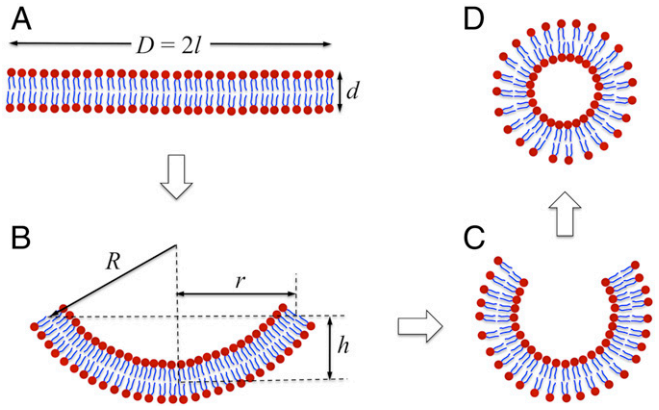

Fig. 1. A schematic illustration of vesicle formation via self-assembly. Driven by hydrophobic interaction along the free edge, a planar circular membrane patch (*A*) curves into a spherical cap (*B* and *C*) and eventually closes to form a vesicle (*D*). Only cross-sections are presented for clarity.

planar membrane patch turns into a closed vesicle. The total system energy at an arbitrary intermediate state can be written as (34)

$$E=\frac{1}{2}\kappa_b\int_A(2H-c_o)^2dA+\kappa_G\int_A K\,dA+\int_A\left(\kappa_1H^4+\kappa_2H^2K+\kappa_3K^2\right)dA+\int_s\gamma ds, \quad [1]$$

where H, K, and c_0 are the mean curvature (the average of the two principal curvatures), Gaussian curvature (the product of the principal curvatures), and spontaneous curvature, respectively. Spontaneous curvature is the natural curvature of the membrane under which there is no internal bending resistance. A nonzero spontaneous curvature may arise from unequal amphiphile numbers, asymmetric lipid compositions (39), or geometrically asymmetric insertion of other molecules (e.g., proteins) between the two constituent layers (40, 41). The first two terms in Eq. **1** account for the linear bending elasticity, where κ_b and κ_G are the bending stiffness and Gaussian bending stiffness, respectively. The third term accounts for the nonlinear bending elasticity, where κ_1, κ_2, and κ_3 are fourth-order moduli. The last term is the line energy along the free edge, where γ is the line tension. Considering an initially planar membrane patch with a diameter of $D=2l$, as shown in Fig. 1*A*, the integrations in Eq. **1** can be carried out to obtain the system energy,

$$E=\frac{1}{2}\pi\kappa_b\cdot\left(\frac{4h}{l}-lc_0\right)^2+4\pi\kappa_G\cdot\left(\frac{h}{l}\right)^2+\frac{16\pi B}{l^2}\cdot\left(\frac{h}{l}\right)^4+2\pi\sqrt{l^2-h^2}\cdot\gamma, \quad [2]$$

where $h\in[0,l]$ is the height of the spherical cap that effectively indicates vesicle shape evolution ($h=0$ corresponds to a planar patch; $h=l$ corresponds to a spherical vesicle), and $B=\kappa_1+\kappa_2+\kappa_3$. In the foregoing, the membrane is assumed to maintain a uniform curvature, and it is assumed that the number of amphiphiles remains constant during vesiculation.

For an initially flat, circular patch ($h=0$), the system energy in Eq. **2** reduces to $E_1=2\pi l\gamma$. For a fully vesiculated sphere ($h=l$), Eq. **2** reduces to: $E_2=8\pi\kappa_b+4\pi\kappa_G+16\pi B/l^2$. Note that the spontaneous curvature is taken as zero ($c_0=0$). To transition from the flat patch configuration into a spherical vesicle, it is necessary that $E_2\le E_1$. It is known that, for phospholipids, $\kappa_G\approx-\kappa_b$ (42). For the case of linear elasticity ($B=0$), the lower bound on the circular membrane patch size that can possibly form a spherical vesicle is given by $l^*=2\kappa_b/\gamma$.

However, this characteristic size does not necessarily define the lower bound of the vesicle size, because energy barriers that could obstruct spontaneous transition may exist between the initial and final configurations. Therefore, let $l = al^*$, where the scaling parameter $a \geq 1$. Defining an additional characteristic length scale $l_c = \sqrt{B/\kappa_b}$ allows the general energy in Eq. **2** to be rewritten as

$$E = 4\pi\kappa_b \left[\left(\frac{h}{al^*}\right)^2 - hc_0 + \frac{1}{8}(al^* c_0)^2 + \frac{4l_c^{\,2}}{(al^*)^2}\left(\frac{h}{al^*}\right)^4 + a\sqrt{1-\left(\frac{h}{al^*}\right)^2} \right], \quad [3]$$

where $h/al^* \in [0,1]$. The characteristic length l_c is associated with nonlinear bending energy and is directly related to membrane thickness (30). The total bending energy of a closed vesicle increases with an increase in l_c, whereas it reduces to linear bending energy as l_c approaches zero. For a given value of l_c, the effect of nonlinear elasticity on bending becomes increasingly dominant with the decrease in membrane size.

Fig. 2 shows the effect of initial membrane size on vesicle formation, including model predictions for linear and nonlinear bending elasticity. Fig. 2*A* shows the normalized total system energy as the membrane configuration changes from a planar patch to a closed vesicle. Here, when the scaling parameter a is close to 1 (near the characteristic patch size), an energy barrier exists as the membrane configuration evolves from planar to spherical. In particular, nonlinearity (denoted by the solid curves in Fig. 2*A*) introduces a significant energy penalty in the later stage of vesiculation. The energy barrier of vesiculation, ΔE, is defined as the difference between the peak energy level and the initial energy level. When a local energy minimum exists at an intermediate configuration between planar and spherical, the energy level at the local minimum is used as the reference energy level to calculate the energy barrier. The energy barrier decreases as the membrane patch size increases, as shown in Fig. 2*B*, until it completely vanishes beyond a critical membrane size: $l = a_c l^*$, where a_c is the critical scaling parameter. However, note that a local energy minimum exists at $0 < h/al^* < 0.6$ when $2 < a < a_c$, indicating the existence of metastable configurations such as cup-shaped open vesicles (Fig. 2*C*).

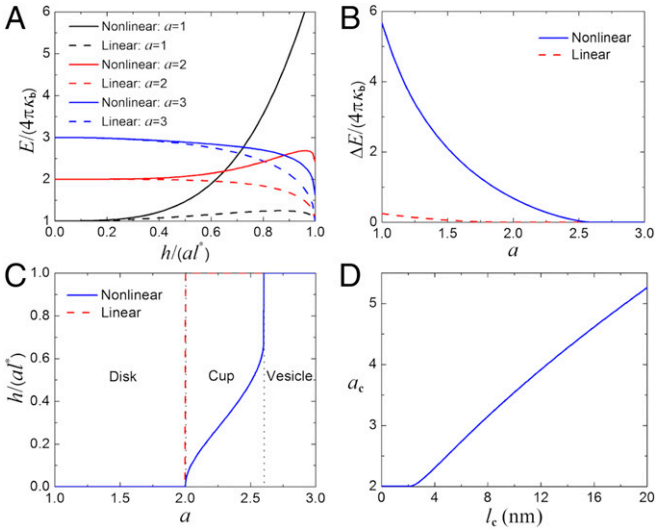

Fig. 2. Effects of membrane patch size on vesiculation. (*A*) System energy profiles as a function of the vesiculation level for membrane patches of different sizes. (*B*) The energy barrier of vesiculation as a function of the membrane patch size. (*C*) Vesiculation geometric configurations as a function of the membrane patch size. (*D*) Critical membrane size as a function of characteristic length associated with nonlinear membrane elasticity.

Table 1. Comparison of vesicle diameter predicted by Eq. 5 with that observed in experiments reported in refs. 15 and 44–46

Vesicle type	d_0, nm	d, nm	D_{min}, nm	D_{ave} from experiments, nm (ref.)
Egg lecithin	4.8	6.2	17.3	21.8 (44)
DMPC	2.65	4.45	13.4	16.8 (45)
PEO_{40}-PEE_{37} (OE7)	8.0	18.6	127.5	176 (15)
PEO_{26}-PBD_{46} (OB2)	9.6	17.6	96.3	132 (46)

Information pertaining to the geometric configurations for egg lecithin, DMPC, and block copolymers (OE7 and OB2) was obtained from refs. 67 and 68.

The linear elasticity model predicts either a disk ($a < 2$) or a full vesicle ($a \geq 2$) configuration, as seen from the dashed line in Fig. 2*C*. Therefore, our approach of incorporating nonlinear elasticity into the bending energy rationalizes experimental observations of open vesicles (25–27). As full vesicles are expected to form spontaneously for only membrane patches larger than the critical size ($l \geq a_c l^*$), the assumption of area conservation allows us to identify the lower bound of the outer diameter of spontaneously self-assembled vesicles as

$$D_{min} = a_c l^* + d = \frac{2a_c\kappa_b}{\gamma} + d, \quad [4]$$

where d is the thickness of the membrane bilayer. As shown in Fig. 2*D*, the critical membrane size scales nearly linearly with the characteristic length associated with nonlinear elasticity ($a_c \propto l_c$ for $l_c > 2$). Treating the hydrophobic tails of the amphiphiles as freely jointed polymers (43), the membrane bending stiffness scales quadratically with membrane thickness, $\kappa_b = K_A d^2/24$. The area compression modulus K_A scales directly with interfacial tension Σ as $K_A = 6\Sigma = 6\gamma/d_0$, where d_0 is the length of the hydrophobic core of the membrane. Therefore, the lower bound in Eq. **4** can be rewritten as

$$D_{min} = \frac{a_c d^2}{2d_0} + d. \quad [5]$$

As the critical scaling parameter is fully determined by the characteristic length associated with nonlinear elasticity, the lower bound of the outer diameter of spontaneously self-assembled vesicles positively correlates with the membrane thickness.

Table 1 shows the comparison between predicted lower bound and the average vesicle sizes for different amphiphiles. Phospholipid bilayer membranes typically have a hydrophobic core of ~3 nm and overall membrane thickness of ~5 nm, yielding a lower bound of spontaneously self-assembled vesicles of ~15.5 nm in diameter (44, 45). By contrast, amphiphilic block copolymers typically have a much longer contour length and can self-assemble into much thicker bilayer membranes and, consequently, into vesicles that are an order of magnitude larger than phospholipid vesicles. These trends predicted by our analysis have been observed in experiments (15, 46). The lower bound given by Eq. **5** is always smaller than the average diameter of self-assembled vesicles and offers a reasonable approximation of the vesicle size.

A nonzero spontaneous curvature may be present when the symmetry between the two constituent layers is broken. An example of such a situation could arise from unequal numbers of lipid molecules in the two layers, which results in a surface area mismatch between outer and inner layers and consequently a

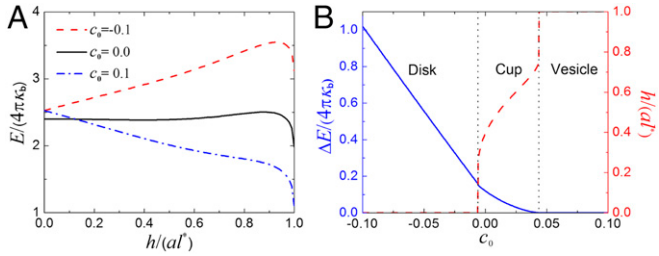

Fig. 3. Effects of spontaneous curvature on vesiculation ($a = 2.4$). (*A*) System energy profiles as a function of the vesiculation level for membrane patches with different spontaneous curvatures. (*B*) The energy barrier and corresponding vesiculation level as a function of the spontaneous curvature.

spontaneous curvature of $c_0 = [2\pi(N_{out} - N_{in})]/[d(N_{out} + N_{in})]$, where N_{out} and N_{in} are the number of lipid molecules in outer and inner layers, respectively. Given a membrane patch smaller than the critical membrane size (Fig. 3*A*), a positive spontaneous curvature (the same curving direction as the spherical surface, $c_0 > 0$) lowers the energy barrier and can even lead to spontaneous vesiculation. On the other hand, a negative spontaneous curvature (the opposite curving direction as the spherical surface, $c_0 < 0$) contributes to an even higher energy barrier, making vesicle formation harder. As shown in Fig. 3*B*, the energy barrier decreases with the increase in spontaneous curvature and could lead to spontaneous vesicle formation at high values of c_0. Note that, in general, a bilayer membrane patch has the flexibility to curve toward both sides, and thus an initial geometric asymmetry always poses a positive spontaneous curvature and promotes vesiculation. Our analysis suggests that increasing spontaneous curvature via flip-flops would be energetically motivated during vesiculation. However, amphiphile molecule exchange across the bilayer typically involves a high energy barrier and therefore rarely happens without assisting molecules (flippases and floppases, ceramide, etc.) (47). On the other hand, similar to water pores, the membrane free edge offers greater flexibility for molecule transport between leaflets (48). Therefore, flip-flops along the free edge are a more likely pathway for lipid exchange across the bilayer, which offers physical insights into the structural asymmetry between the inner and outer layers of self-assembled vesicles, which has been observed in MD simulations (48).

The interrelated effects of the membrane patch size and spontaneous curvature on vesiculation are shown in Fig. 4. Fig. 4*A* is a plot of the normalized energy barrier ΔE as a function of patch size a and spontaneous curvature c_0. The energy barrier decreases with the increase in both membrane patch size and spontaneous curvature. The vesiculation level is also identified in the space of membrane patch size and spontaneous curvature (Fig. 4*B*). The phase diagram allows us to predict the final configuration of an initially flat membrane with a certain spontaneous curvature. Stable cup-shaped open vesicles are formed when the membrane patch size is smaller than the critical membrane size, which decreases as the spontaneous curvature increases. The transition from "cup" to "vesicle" is much sharper than the transition from "disk" to "cup," indicating that vesicle closure is energetically favored.

Vesicle Size Distribution

Although the lower bound of the vesicle size is determined by the energetics, the upper bound is mainly limited by entropic effects. Therefore, to probe the size distribution of self-assembled vesicles, it becomes essential to accurately characterize system entropy. Prior studies (24, 49) estimated vesicle size distributions by invoking the assumption that amphiphiles self-assemble into a fixed number of vesicles. Configurations including disks and cup-shaped open vesicles were not taken into consideration. Such an approach largely underestimates the configurational entropy of the self-assembling system. To include all possible configurations, we let $n_{m,h}$ denote the number of membrane patches consisting of $m \in [1, M]$ amphiphiles with a dome height of $h \in [0, 2R_s]$, where M is the number of amphiphiles in the largest membrane patch and $R_s = \sqrt{mA_0/8\pi}$ is the radius of the corresponding closed vesicle, where A_0 is the area per amphiphile. The total number of amphiphiles is given by $N = \sum_{m=1}^{M} m(\sum_{h=0}^{2R_s} n_{m,h})$. The total free energy functional can be written as

$$G = \sum_{m=1}^{M}\sum_{h=0}^{2R_s} n_{m,h}C_{m,h}\gamma + \sum_{m=1}^{M}\sum_{h=0}^{2R_s} n_{m,h}\left[\left(\frac{2\kappa_b}{R^2} + \frac{\kappa_G}{R^2} + \frac{B}{R^4}\right)\frac{mA_0}{2} - \frac{\alpha}{2}k_BT\ln\frac{m}{2}\right] - k_BT\left[N\ln N - \sum_{m=1}^{M}\sum_{h=0}^{2R_s}(mn_{m,h})\ln(mn_{m,h})\right] - k_BTN\ln\varphi, \quad [6]$$

where

$$\alpha = \frac{12 + \frac{30l_c^2}{R^2}}{1 + \frac{3l_c^2}{R^2} + \sqrt{1 + \frac{6l_c^2}{R^2} + \frac{9l_c^4}{R^4} + \frac{3mk_BTl_c^2}{2\kappa_bR^2}}}, \quad [7]$$

where $C_{m,h}$ denotes the perimeter of the free edge of the membrane patches consisting of m amphiphiles with a dome height of h. The first two terms are energetic contributions: The first term is the line energy from free edge, whereas the second term accounts for the renormalized bending energy after taking membrane fluctuation into consideration (37); here, k_B and T are the Boltzmann constant and temperature, respectively. The third and fourth terms are entropic contributions: The third term is the configurational entropy, and the fourth term accounts for the entropy associated with dispersing N amphiphiles into aqueous solution, where φ is the volume fraction of amphiphiles (50).

Minimizing the total free energy functional with respect to the independent variable $n_{m,h}$ yields the membrane patch size distribution

$$n_{m,h} = \frac{N\varphi}{m}\exp\left\{-\left[C_{m,h}\gamma + \left(\frac{2\kappa_b}{R^2} + \frac{\kappa_G}{R^2} + \frac{B}{R^4}\right)\frac{mA_0}{2} - \frac{\alpha}{2}k_BT\ln\frac{m}{2}\right]\Big/(k_BTm)\right\}. \quad [8]$$

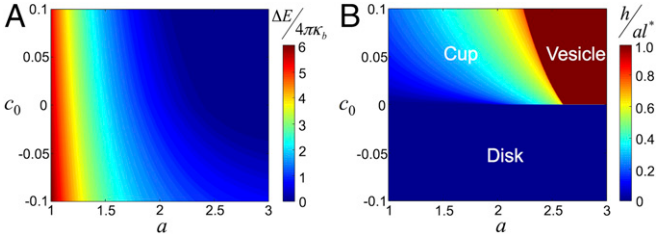

Fig. 4. Interrelated effects of membrane size and spontaneous curvature on vesiculation. (*A*) Normalized energy barrier and (*B*) geometric configuration of vesiculation as a function of membrane patch size and spontaneous curvature.

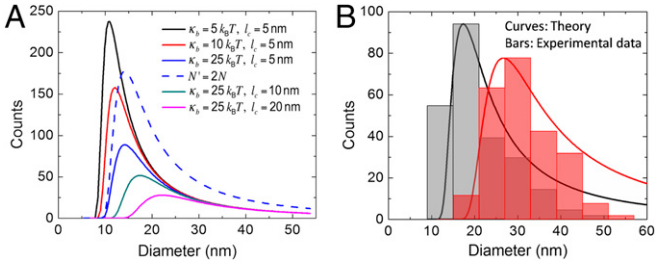

Fig. 5. Size distribution of self-assembled vesicles. (*A*) Vesicle size distribution with varying bending stiffness, nonlinearity characteristic length scale, and total number of amphiphiles. The dashed curve has the stiffness of $\kappa_b = 25\ k_BT$ and nonlinearity characteristic length scale of $l_c = 5$ nm. (*B*) Overlying theoretical fitting with experimental data reproduced from ref. 44. The parameters used in the analysis are ($\kappa_b = 12\ k_BT$, $l_c = 10$ nm) and ($\kappa_b = 36\ k_BT$, $l_c = 16$ nm) for pure egg lecithin (black) and egg lecithin/cholesterol (red) vesicles, respectively.

The vesicle size distribution can be readily obtained by substituting $h = 2R_s$ into Eq. **8**, which yields

$$n_{m,2R_s} = \frac{N\varphi}{m}\exp\left[-\frac{4\pi\kappa_b}{mk_BT}\left(1+\frac{8\pi l_c^2}{mA_0}\right)+\frac{\alpha}{2m}\ln\frac{m}{2}\right]. \qquad [9]$$

As shown in Fig. 5*A*, the vesicle size distribution features a sharp rise immediately above the minimum critical vesicle size, and a long tail as the vesicle size increases. Such a positively skewed distribution is consistent with experimental measurements (44, 45). A stiff membrane diminishes the formation of small vesicles such that both the cutoff diameter and peak diameter increase with the increase in membrane bending stiffness. Because the nonlinearity in membrane elasticity essentially imposes an extra bending resistance to small vesicle formation, increasing the nonlinearity increases the cutoff vesicle size more effectively. However, membrane stiffness and nonlinear elasticity have little impact on the formation of large vesicles (>35 nm). The size distribution linearly scales with the total number of amphiphiles, but the cutoff size and peak diameter remain unchanged, which has been experimentally confirmed (51).

As an illustration of this line of reasoning, we compare the predicted vesicle size distribution with experimental data (44), where egg lecithin vesicles were synthesized under sonication. As shown in Fig. 5*B*, the presence of cholesterol (egg lecithin/cholesterol = 60%/40%) shifts the size distribution to the right and makes the distribution broader. Pure egg lecithin membrane (52) has a bending stiffness of $\sim 12\ k_BT$. However, cholesterol induces a threefold increase in membrane stiffness (53) and can increase the membrane thickness by more than 20%, due to its condensing effect in lipid bilayers (54, 55). Membrane thickening in the presence of cholesterol is responsible for enhanced nonlinearity in membrane bending. Our vesicle size distribution analysis (solid lines in Fig. 5*B*) is able to effectively capture the increases in vesicle peak size and distribution width by considering the simultaneous increase in membrane bending stiffness and thickness (i.e., nonlinearity).

Discussion and Conclusion

Our energetic and thermodynamic analyses, which included the higher-order energy terms in membrane bending, enabled us to identify the essential role of membrane thickness, a missing component in the linear elastic membrane model (56), in mediating vesicle configuration and size distribution. Although the concept of nonlinear elasticity in membrane bending and its implications for vesiculation have been topics of discussion for some time (31, 49), previous theoretical studies of membrane mechanics in the context of living cells and microsized artificial fluid vesicles have typically analyzed membrane bending by effectively treating (56) the membrane as a zero-thickness sheet undergoing linear elastic, small deformation. The accuracy of such a linear elastic model becomes questionable whenever the local radius of curvature becomes comparable to the membrane thickness (29, 33). Under these circumstances, it is necessary to incorporate nonlinear elasticity effects to account for the associated significant membrane stiffening (32, 34, 37).

One of the main limitations of the linear elastic membrane model is that it only allows for disk-like planar membrane patches and closed vesicles as stable configurations in a self-assembling system (23, 24, 49), although stable cup-shaped open vesicles have been observed in several experimental studies (25–27). Our energy-based analysis, incorporating nonlinear elasticity, indicates that those cup-shaped open vesicles are stabilized by the additional bending resistance arising particularly in the later stage of vesiculation as the radius of curvature approaches the membrane thickness.

Our analysis also shows that the critical membrane size for spontaneous vesiculation correlates with membrane thickness. The range of membrane thickness for different types of phospholipids is very limited. Therefore, the predicted lower bound on the diameter of phospholipid vesicles falls in a narrow range of about 10 nm to 20 nm, and is at or slightly below the average vesicle size measured in different experiments (20, 44, 45, 57). In contrast, amphiphile block copolymers are synthesized via polymerization, where both the hydrophilic and hydrophobic chains can vary dramatically, and vesicle diameters range from around 100 nm to several micrometers (7, 58). In these circumstances, our predication on the lower bound of vesicle size can potentially serve as a guideline to help select specific designs of block copolymers that facilitate the formation of larger vesicles, desired for optimal performance. In addition, our nonlinear analysis shows that the structural asymmetry between the two constituent layers always promotes vesiculation by reducing the critical membrane size for spontaneous vesicle formation.

Membrane stiffness and bilayer thickness are identified here as two important factors that mediate vesicle size distribution. Membrane stiffness is a linear elasticity concept, whereas the membrane thickness is related to the characteristic length associated with nonlinear bending energy. Therefore, they are considered as two separate parameters. Changes in the membrane thickness may or may not result in changes in the bending stiffness, depending on whether there are also changes in membrane composition. Increasing membrane stiffness and membrane thickness would promote the formation of larger vesicles. The size distribution predicted by our analyses is found to be in good agreement with experimental observations where sonication is performed to fully disperse amphiphiles. In fact, the peak size of self-assembled vesicles can vary significantly from sub-10 nm to hundreds of nanometers, and is dependent upon the technique adopted, even for the same type of lipids (45). It was found (45) that the peak size of dimyristoylphosphatidylcholine (DMPC) vesicles effectively decreased with the increase in sonication time. Large vesicles may readily form from large membrane fragments that are not fully dispersed in aqueous solution or coalescence of small fragments (38). Future studies may account for the initial dispersion level of amphiphiles and fusion among membrane fragments to fully capture the self-assembly process.

In addition to providing a comprehensive physical understanding of vesicle formation, the framework presented here may be readily adapted to help elucidate the biophysical and biomechanical features of physiologically relevant EVs, such as exosomes. Exosomes are currently emerging as a new liquid biopsy tool, because they harbor proteins, long and short RNAs, lipids, and/or metabolites that are specific to their tissue of origin. A better definition of the biophysical and biomechanical features of exosomes may promote new applications of EV-based liquid biopsies. For example, it has been shown that exosomes secreted from cancer cells are smaller than those secreted from healthy cells (59). This difference may point to several potentially useful avenues for cancer diagnostics: (*i*) The size difference may allow for vesicle sorting using such methods as standing surface acoustic wave technique (60, 61) to separate the vesicles secreted from tumor cells and those from

healthy cells, providing a possible novel approach for cancer diagnosis; and (*ii*) smaller tumor vesicles suggest a lower membrane stiffness, consistent with the observations that the stiffness of individual cancer cells in most cancers is lower than that of healthy cells (62–64). It is also noted that synthetic small unilamellar vesicles have been studied extensively as potential drug carriers for cancer treatment, and their advantages over other drug delivery platforms have been highlighted (2, 65, 66). Our analyses thus indicate potential pathways for manipulating vesicle configuration and size for more effective cargo delivery that could have implications for clinical use.

ACKNOWLEDGMENTS. Research reported in this publication was supported by Eunice Kennedy Shriver National Institute of Child Health and Human Development Grant R01HD086325. C.H., D.Q., S.S., and K.J.H. also acknowledge financial support from Carnegie Mellon University.

1. Torchilin VP (2007) Micellar nanocarriers: Pharmaceutical perspectives. *Pharm Res* 24(1):1–16.
2. Allen TM, Cullis PR (2013) Liposomal drug delivery systems: From concept to clinical applications. *Adv Drug Deliv Rev* 65(1):36–48.
3. Pisitkun T, Shen R-F, Knepper MA (2004) Identification and proteomic profiling of exosomes in human urine. *Proc Natl Acad Sci USA* 101(36):13368–13373.
4. Donker RB, et al. (2012) The expression profile of C19MC microRNAs in primary human trophoblast cells and exosomes. *Mol Hum Reprod* 18(8):417–424.
5. Mann S (2009) Self-assembly and transformation of hybrid nano-objects and nanostructures under equilibrium and non-equilibrium conditions. *Nat Mater* 8(10):781–792.
6. Holmberg K, Jonsson B, Kronberg B, Lindman B (2002) Surfactants and Polymers in Aqueous Solution (Wiley, Chichester, UK).
7. Kita-Tokarczyk K, Grumelard J, Haefele T, Meier W (2005) Block copolymer vesicles—Using concepts from polymer chemistry to mimic biomembranes. *Polymer* 46(11):3540–3563.
8. Šegota S, Tezak D (2006) Spontaneous formation of vesicles. *Adv Colloid Interface Sci* 121(1-3):51–75.
9. Valadi H, et al. (2007) Exosome-mediated transfer of mRNAs and microRNAs is a novel mechanism of genetic exchange between cells. *Nat Cell Biol* 9(6):654–659.
10. Delorme-Axford E, et al. (2013) Human placental trophoblasts confer viral resistance to recipient cells. *Proc Natl Acad Sci USA* 110(29):12048–12053.
11. Robbins PD, Morelli AE (2014) Regulation of immune responses by extracellular vesicles. *Nat Rev Immunol* 14(3):195–208.
12. Hoshino A, et al. (2015) Tumour exosome integrins determine organotropic metastasis. *Nature* 527(7578):329–335.
13. Ouyang Y, et al. (2016) Isolation of human trophoblastic extracellular vesicles and characterization of their cargo and antiviral activity. *Placenta* 47:86–95.
14. Antonietti M, Forster S (2003) Vesicles and liposomes: A self-assembly principle beyond lipids. *Adv Mater* 15(16):1323–1333.
15. is Lee JC, et al. (2001) Preparation, stability, and in vitro performance of vesicles made with diblock copolymers. *Biotechnol Bioeng* 73(2):135–145.
16. Zhang S, Li J, Lykotrafitis G, Bao G, Suresh S (2009) Size-dependent endocytosis of nanoparticles. *Adv Mater* 21(4):419–424.
17. Yi X, Shi X, Gao H (2011) Cellular uptake of elastic nanoparticles. *Phys Rev Lett* 107(9): 098101.
18. Huang C, Zhang Y, Yuan H, Gao H, Zhang S (2013) Role of nanoparticle geometry in endocytosis: Laying down to stand up. *Nano Lett* 13(9):4546–4550.
19. Mulcahy LA, Pink RC, Carter DRF (2014) Routes and mechanisms of extracellular vesicle uptake. *J Extracell Vesicles* 3:1–14.
20. Peter Fromherz CR and DR (1986) From discoid micelles to spherical vesicles. The concept of edge activity. *Faraday Discuss Chem Soc* 81:39–48.
21. Noguchi H, Gompper G (2006) Dynamics of vesicle self-assembly and dissolution. *J Chem Phys* 125(16):164908.
22. Yuan H, Huang C, Li J, Lykotrafitis G, Zhang S (2010) One-particle-thick, solvent-free, coarse-grained model for biological and biomimetic fluid membranes. *Phys Rev E Stat Nonlin Soft Matter Phys* 82(1 Pt 1):011905.
23. Boal DH, Rao M (1992) Topology changes in fluid membranes. *Phys Rev A* 46(6):3037–3045.
24. Guida V (2010) Thermodynamics and kinetics of vesicles formation processes. *Adv Colloid Interface Sci* 161(1-2):77–88.
25. Hamada T, Sugimoto R, Vestergaard MC, Nagasaki T, Takagi M (2010) Membrane disk and sphere: Controllable mesoscopic structures for the capture and release of a targeted object. *J Am Chem Soc* 132(30):10528–10532.
26. Saitoh A, Takiguchi K, Tanaka Y, Hotani H (1998) Opening-up of liposomal membranes by talin. *Proc Natl Acad Sci USA* 95(3):1026–1031.
27. Shioi A, Hatton TA (2002) Model for formation and growth of vesicles in mixed anionic/cationic (SOS/CTAB) surfactant systems. *Langmuir* 18(20):7341–7348.
28. Vauthey S, Santoso S, Gong H, Watson N, Zhang S (2002) Molecular self-assembly of surfactant-like peptides to form nanotubes and nanovesicles. *Proc Natl Acad Sci USA* 99(8):5355–5360.
29. Shinoda W, Nakamura T, Nielsen SO (2011) Free energy analysis of vesicle-to-bicelle transformation. *Soft Matter* 7(19):9012–9020.
30. Harmandaris VA, Deserno M (2006) A novel method for measuring the bending rigidity of model lipid membranes by simulating tethers. *J Chem Phys* 125(20):204905.
31. Fromherz P (1983) Lipid-vesicle structure: Size control by edge-active agents. *Chem Phys Lett* 94(3):259–266.
32. Nakamura T, Shinoda W (2013) Method of evaluating curvature-dependent elastic parameters for small unilamellar vesicles using molecular dynamics trajectory. *J Chem Phys* 138(12):124903.
33. Manyuhina OV, et al. (2007) Anharmonic magnetic deformation of self-assembled molecular nanocapsules. *Phys Rev Lett* 98(14):146101.
34. Li J, Pastor KA, Shi AC, Schmid F, Zhou J (2013) Elastic properties and line tension of self-assembled bilayer membranes. *Phys Rev E Stat Nonlin Soft Matter Phys* 88(1):012718.
35. Fournier JB, Galatola P (1997) Tubular vesicles and effective fourth-order membrane elastic theories. *Europhys Lett* 39(2):225–230.
36. Li J, Zhang H, Qiu F, Shi AC (2013) Emergence and stability of intermediate open vesicles in disk-to-vesicle transitions. *Phys Rev E Stat Nonlin Soft Matter Phys* 88(1):012719.
37. Ahmadpoor F, Sharma P (2016) Thermal fluctuations of vesicles and nonlinear curvature elasticity—Implications for size-dependent renormalized bending rigidity and vesicle size distribution. *Soft Matter* 12(9):2523–2536.
38. Weiss TM, et al. (2005) Dynamics of the self-assembly of unilamellar vesicles. *Phys Rev Lett* 94:038303.
39. Safran SA, Pincus P, Andelman D (1990) Theory of spontaneous vesicle formation in surfactant mixtures. *Science* 248(4953):354–356.
40. Różycki B, Lipowsky R (2015) Spontaneous curvature of bilayer membranes from molecular simulations: Asymmetric lipid densities and asymmetric adsorption. *J Chem Phys* 142(5):054101.
41. Döbereiner HG, Selchow O, Lipowsky R (1999) Spontaneous curvature of fluid vesicles induced by trans-bilayer sugar asymmetry. *Eur Biophys J* 28(2):174–178.
42. Hu M, Briguglio JJ, Deserno M (2012) Determining the Gaussian curvature modulus of lipid membranes in simulations. *Biophys J* 102(6):1403–1410.
43. Rawicz W, Olbrich KC, McIntosh T, Needham D, Evans E (2000) Effect of chain length and unsaturation on elasticity of lipid bilayers. *Biophys J* 79(1):328–339.
44. Van Venetië R, Leunissen-Bijvelt J, Verkleij AJ, Ververgaert PHJT (1980) Size determination of sonicated vesicles by freeze-fracture electron microscopy, using the spray-freezing method. *J Microsc* 118(4):401–408.
45. Maulucci G, et al. (2005) Particle size distribution in DMPC vesicles solutions undergoing different sonication times. *Biophys J* 88(5):3545–3550.
46. Yewle J, Wattamwar P, Tao Z, Ostertag EM, Ghoroghchian PP (2016) Progressive saturation improves the encapsulation of functional proteins in nanoscale polymer vesicles. *Pharm Res* 33(3):573–589.
47. Contreras FX, Sánchez-Magraner L, Alonso A, Goñi FM (2010) Transbilayer (flip-flop) lipid motion and lipid scrambling in membranes. *FEBS Lett* 584(9):1779–1786.
48. de Vries AH, Mark AE, Marrink SJ (2004) Molecular dynamics simulation of the spontaneous formation of a small DPPC vesicle in water in atomistic detail. *J Am Chem Soc* 126(14):4488–4489.
49. Helfrich W (1986) Size distributions of vesicles: The role of the effective rigidity of membranes. *J Phys* 47(2):321–329.
50. Yuan H, Huang C, Zhang S (2010) Virus-inspired design principles of nanoparticle-based bioagents. *PLoS One* 5(10):e13495.
51. Kölchens S, Ramaswami V, Birgenheier J, Nett L, O'Brien DF (1993) Quasi-elastic light scattering determination of the size distribution of extruded vesicles. *Chem Phys Lipids* 65(1):1–10.
52. Cuvelier D, Derényi I, Bassereau P, Nassoy P (2005) Coalescence of membrane tethers: Experiments, theory, and applications. *Biophys J* 88(4):2714–2726.
53. Waugh RE, Song J (1991) Measurements of membrane bending stiffness: Contributions from intrinsic monolayer stiffness and monolayer coupling. *Period Biol* 93(2):217–222.
54. Hung W-C, Lee M-T, Chen F-Y, Huang HW (2007) The condensing effect of cholesterol in lipid bilayers. *Biophys J* 92(11):3960–3967.
55. de Meyer F, Smit B (2009) Effect of cholesterol on the structure of a phospholipid bilayer. *Proc Natl Acad Sci USA* 106(10):3654–3658.
56. Seifert U (1997) Configurations of fluid membranes and vesicles. *Adv Phys* 46(1):13–137.
57. Schurtenberger P, Hauser H (1984) Characterization of the size distribution of unilamellar vesicles by gel filtration, quasi-elastic light scattering and electron microscopy. *Biochim Biophys Acta* 778(3):470–480.
58. Lim Soo P, Eisenberg A (2004) Preparation of block copolymer vesicles in solution. *J Polym Sci Part B Polym Phys* 42:923–938.
59. Zhang W, et al. (2016) Characterization of exosomes derived from ovarian cancer cells and normal ovarian epithelial cells by nanoparticle tracking analysis. *Tumour Biol* 37(3):4213–4221.
60. Ding X, et al. (2014) Cell separation using tilted-angle standing surface acoustic waves. *Proc Natl Acad Sci USA* 111(36):12992–12997.
61. Li P, et al. (2015) Acoustic separation of circulating tumor cells. *Proc Natl Acad Sci USA* 112(16):4970–4975.
62. Swaminathan V, et al. (2011) Mechanical stiffness grades metastatic potential in patient tumor cells and in cancer cell lines. *Cancer Res* 71(15):5075–5080.
63. Xu W, et al. (2012) Cell stiffness is a biomarker of the metastatic potential of ovarian cancer cells. *PLoS One* 7(10):e46609.
64. Lekka M (2016) Discrimination between normal and cancerous cells using AFM. *Bionanoscience* 6(1):65–80.
65. Malam Y, Loizidou M, Seifalian AM (2009) Liposomes and nanoparticles: Nanosized vehicles for drug delivery in cancer. *Trends Pharmacol Sci* 30(11):592–599.
66. Lian T, Ho RJ (2001) Trends and developments in liposome drug delivery systems. *J Pharm Sci* 90(6):667–680.
67. Papahadjopoulos D (1973) Phospholipid membranes as experimental models for biological membranes. *Biological Horizons in Surface Science* (Elsevier, New York), pp 159–225.
68. Photos PJ, Bermudez H, Aranda-Espinoza H, Shillcock J, Discher DE (2007) Nuclear pores and membrane holes: Generic models for confined chains and entropic barriers in pore stabilization. *Soft Matter* 3(3):364–371.